Supplement of The Cryosphere, 17, 371–390, 2023
https://doi.org/10.5194/tc-17-371-2023-supplement

The Cryosphere
Open Access

Supplement of

Impact of icebergs on the seasonal submarine melt of Sermeq Kujalleq

Karita Kajanto et al.

Correspondence to: Karita Kajanto (karita.kajanto@uib.no)

Introduction

This material supports the results, interpretation and conclusions presented in the main text. Fig. S1 presents the Disko Bay boundary conditions for temperature and salinity and the observational data used as a basis to create the synthetic profiles. Table S1 lists the model parameters used in all experiments, while Table 1 shows parameters that vary between experiments. Fig. S2 shows the domain average properties throughout the entirety of the main model runs *NoIBP* and *IBP*, while Fig. S3 shows the mean properties within the iceberg extent in *IBP* for the entire model run, and also separately within three vertical layers. Fig. S4 presents the results of sensitivity experiments on model parameters conducted in the *IBP* setup as the peak-summer mid-fjord properties. Figs. S5 and S6 show the sensitivity experiments that were conducted in the *NoIBP* setup; sensitivity to the hydrostatic assumption (Fig. S5) and sensitivity of plume melt to the initial velocity of the subglacial discharge (Fig. S6). Fig. S7 presents the results from passive tracer experiments that demonstrate the early and late-season refluxing at the sill, as well as the deepening of the GMW outflow in *IBP*.

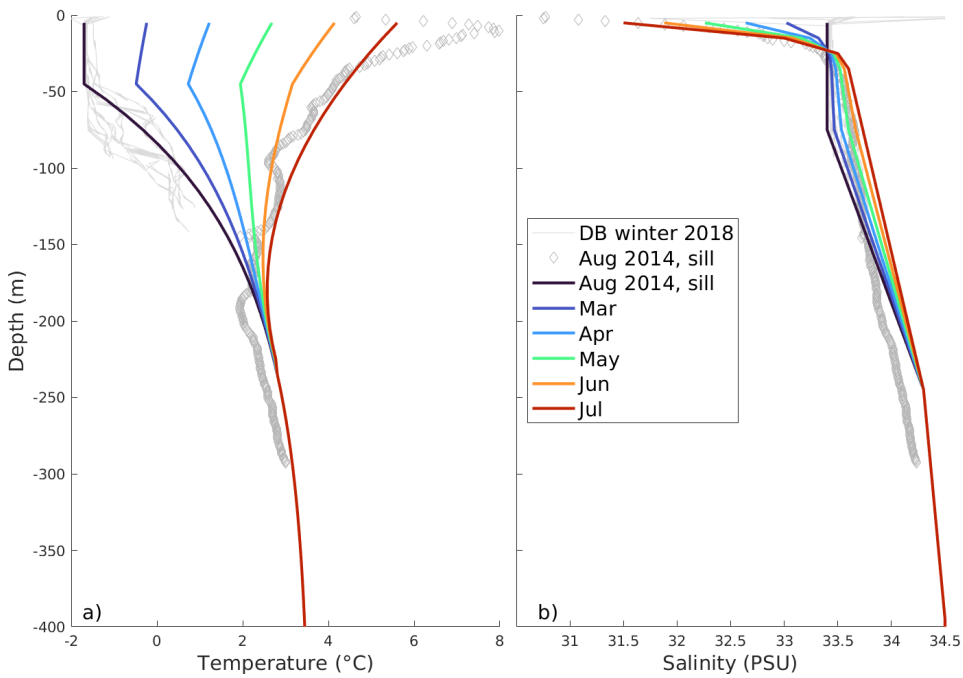

Figure S1. Model temperature (a) and salinity (b) boundary conditions for Disko Bay (colored lines), August 2014 temperature and salinity profiles on Disko Bay next to the sill (grey diamonds) (Beaird et al., 2017), and winter profiles for Disko Bay close to Quequertarsuaq in 2018 (grey lines) (Monitoring, 2020).

Table S1. List of model parameters

Parameter	Value	Unit
Heat capacity of ice	2000	J kg^{-1} $°C^{-1}$
Heat capacity of water	3974	J kg^{-1} $°C^{-1}$
Acceleration due to gravity	9.81	m s^{-2}
Ice temperature	-10	°C
Latent heat of melting	$3.34 * 10^5$	J kg^{-1}
Thermal turbulent transfer coefficient	0.022	
Salt turbulent transfer coefficient	0.00062	
Iceberg drag coefficient	0.0025	
Freezing point slope	-0.0573	°C PSU^{-1}
Freezing point offset	0.0832	°C
Freezing point depth	0.00076	°C m^{-1}
Background velocity, icebergs	0.06	m s^{-1}
Background velocity, plume	0.017	m s^{-1}
Ice density	917	kg m^{-3}
Vertical Laplacian diffusion coefficient of temperature and salinity	$1 * 10^{-5}$	$m^2 s^{-1}$
Horizontal diffusion coefficient of temperature and salinity	20	$m^2 s^{-1}$
Vertical eddy viscosity	$1 * 10^{-5}$	$m^2 s^{-1}$
Smagorinsky non-dimensional viscosity factor	2.2	
Entrainment parameter	0.1	
Reference density	1027	kg m^{-3}
OBCS relaxation timescale, inner boundary	30	d
OBCS relaxation timescale, outer boundary	16.7	h

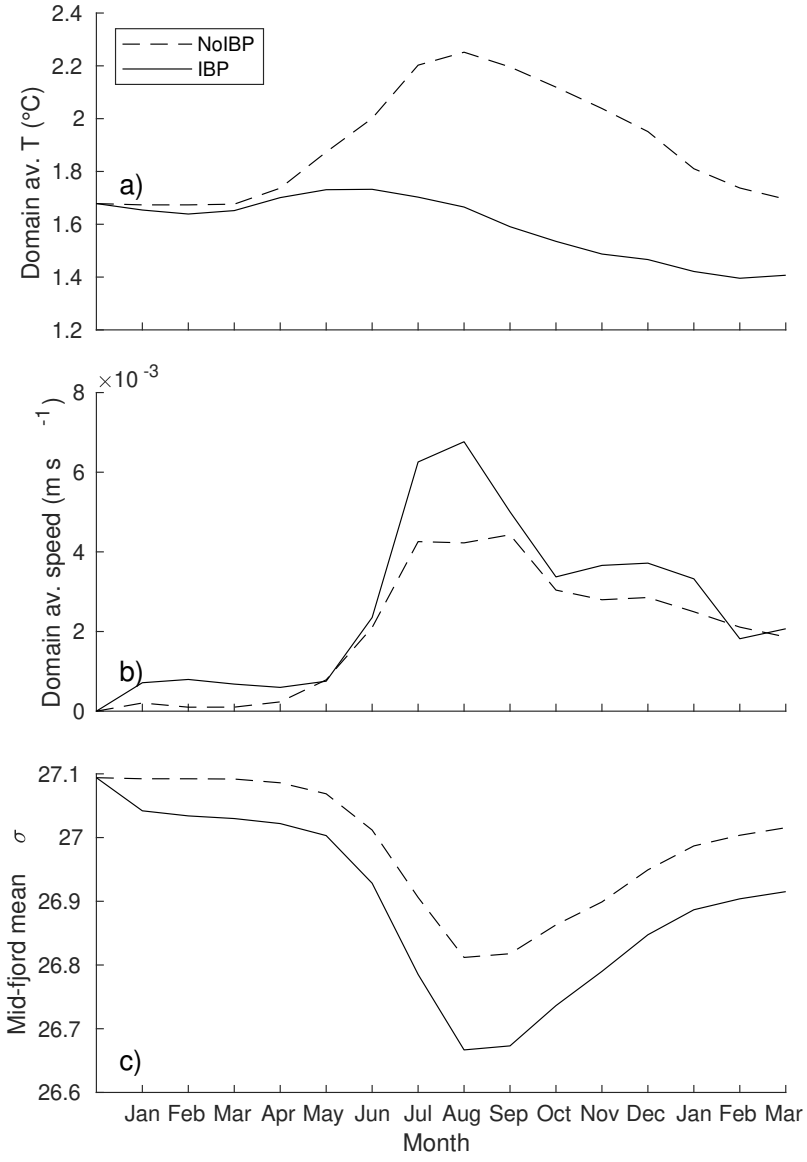

Figure S2. Time evolution throughout the model run of a) domain averaged temperature, b) domain averaged speed and c) vertically averaged potential density at mid-fjord location for experiments with and without icebergs (*IBP* and *NoIBP* respectively).

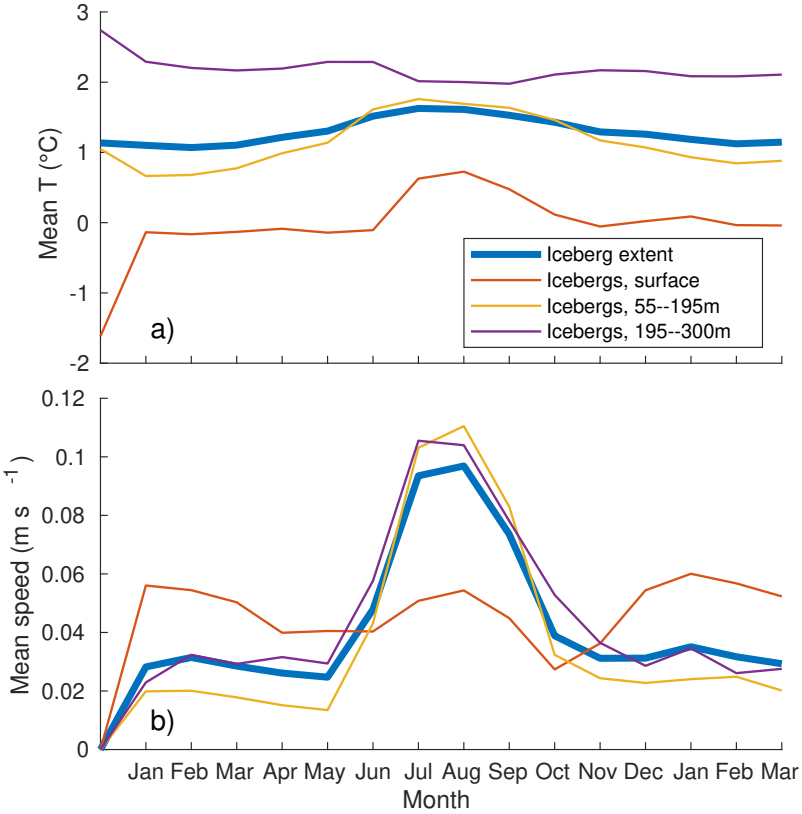

Figure S3. Average temperature (a) and speed of water flow (b) within the extent of the icebergs throughout experiment *IBP*, for the whole iceberg extent (sill to glacier, surface to 300 m depth, as in Fig. 2), surface layer (0–55 m), intermediate layer water roughly within the outflow region (55–195 m), and intermediate water roughly within the inflow region (195–300 m).

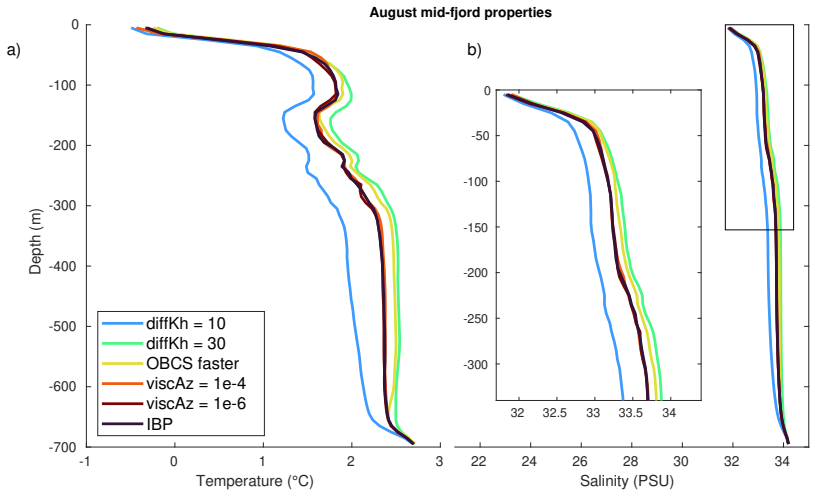

Figure S4. Mid-fjord properties of *IBP* in August (black line) and five sensitivity experiments for IBP: variation of horizontal diffusivity by $\pm 10\ \mathrm{m^2 s^{-1}}$ from the used value of $20\ \mathrm{m^2 s^{-1}}$ (blue and green lines), an order-of-magnitude faster OBCS inner boundary restoration time scale of 3 days (yellow line) and order-of-magnitude variations to the vertical viscosity (orange and brown lines). Surface conditions are not impacted by any of the sensitivity experiments, while the horizontal diffusivity and the restoration time scale have a slight impact to the degree of basin modification.

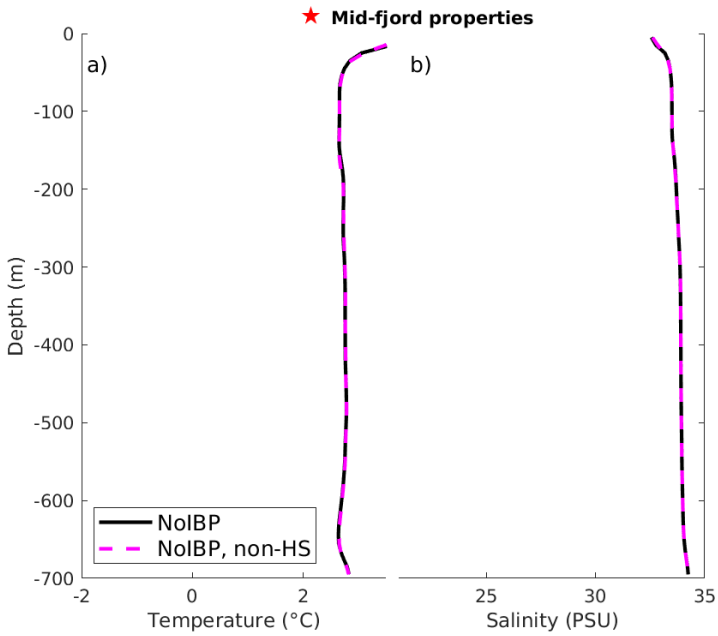

Figure S5. Mid-fjord properties of *NoIBP* in August in assuming hydrostatic mode (black line) vs. non-hydrostatic mode (dashed pink line). Hydrostatic assumptions are used in all experiments due to computational efficiency.

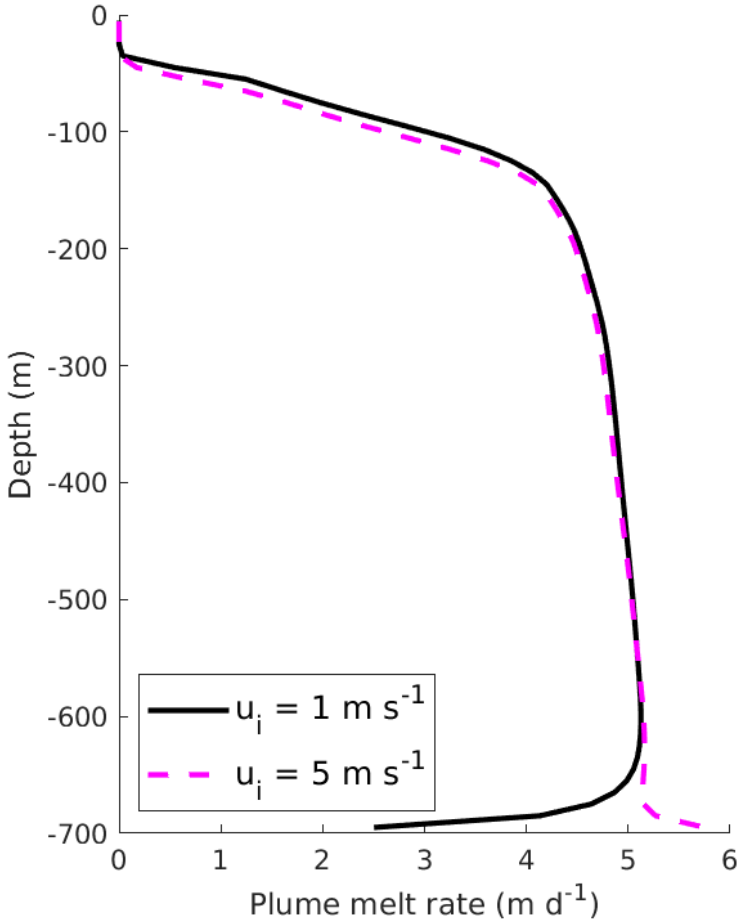

Figure S6. Sensitivity of the plume melt rate of the sheet plume model (Jenkins, 2011) to the choice of intial water velocity for a fixed subglacial discharge in *NoIBP*. Recommended value is 1 m s^{-1} (Cowton et al., 2015) (black solid line), while 5 m s^{-1} is a high-end estimate (pink dashed line). The initial water velocity is kept constant throughout the experiments, while changes in sheet thickness accommodate the increase in subglacial discharge.

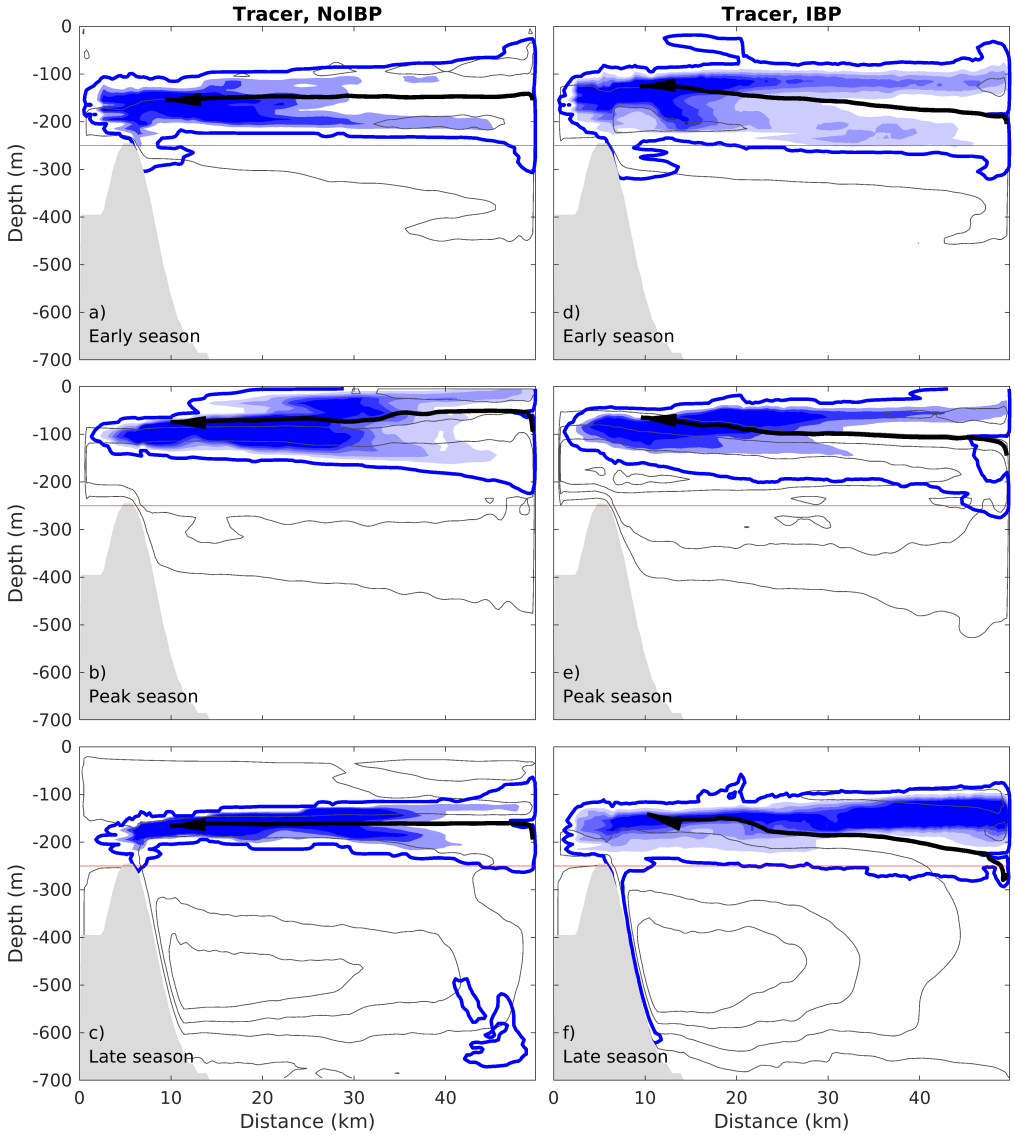

Figure S7. Snapshots of tracer concentration exiting the sill in early (June, a,d), peak (August, b,e) and late (October, c,f) season for both *NoIBP* (a–c) and *IBP* (d–e). A passive tracer pulse is injected into the subglacial discharge at time zero, in order to identify GMW originating from the plume. The snapshot is taken once the tracer reaches the sill, but tracer concentration in the domain is still >90%. Due to different flow speeds this takes place at slightly different duration since the injection. The snapshots are taken: a) 4 d b) 3 d c) 4 d d) 5 d e) 2.5 d and f) 6 d since the injection. The blue contour indicates tracer concentration of 1e-5, and the grey contours streamlines of the horizontal flow rate, as in Fig. 4. The black arrows indicate the centreline of the GMW outflow from the plume, as in Figs. 3 and 4. The red horizontal line represents sill depth of 250 m. Early and late season experiments show refluxing at the sill, while during peak season the relatively shallow GMW outflow exits the fjord entirely. GMW extends 40 m deeper in *IBP* than *NoIBP* in the early season, and 50 m deeper in the peak and late seasons.

References

Beaird, N., Straneo, F., and Jenkins, W.: Characteristics of meltwater export from Jakobshavn Isbræ and Ilulissat Icefjord, Annals of Glaciology, 58, 107–117, https://doi.org/10.1017/aog.2017.19, 2017.

Cowton, T., Slater, D., Sole, A., Goldberg, D., and Nienow, P.: Modeling the impact of glacial runoff on fjord circulation and submarine melt rate using a new subgrid-scale parameterization for glacial plumes, Journal of Geophysical Research: Oceans, 120, 796–812, https://doi.org/10.1002/2014JC010324, 2015.

Jenkins, A.: Convection-driven melting near the grounding lines of ice shelves and tidewater glaciers, Journal of Physical Oceanography, 41, 2279–2294, https://doi.org/10.1175/JPO-D-11-03.1, 2011.

Monitoring, G. E.: MarineBasis Disko - Water column - CTD measurements (Version 1.0) [Data set], https://doi.org/https://doi.org/10.17897/WH30-HT61, 2020.